Mathematical Modeling of Air- and Oxy-Coal Confined Swirling Flames on Two Extended Eddy-Dissipation Models

ARTICLE *in* INDUSTRIAL & ENGINEERING CHEMISTRY RESEARCH · JANUARY 2012

Impact Factor: 2.59 · DOI: 10.1021/ie201430a

8 AUTHORS, INCLUDING:

Jingzhang Liu
Chinese Academy of Sciences
4 PUBLICATIONS **33** CITATIONS
SEE PROFILE

Zhaohui Liu
Huazhong University of Science and Technol…
94 PUBLICATIONS **618** CITATIONS
SEE PROFILE

I&EC research
Industrial & Engineering Chemistry Research

ARTICLE

pubs.acs.org/IECR

Mathematical Modeling of Air− and Oxy−Coal Confined Swirling Flames on Two Extended Eddy-Dissipation Models

Jingzhang Liu, Sheng Chen, Zhaohui Liu,* Ke Peng, Nan Zhou, Xiaohong Huang, Tai Zhang, and Chuguang Zheng

State Key Laboratory of Coal Combustion, Huazhong Univeristy of Science and Technology, 1037 Luoyu Road, Wuhan, Hubei, People's Republic of China

ABSTRACT: The mathematical modeling of air− and oxy−coal flames is a great challenge because of the complexity of the turbulence chemistry interactions. However, the different turbulence chemistry interaction models can give very different results. Therefore, an investigation of the effects of these interactions on air− and oxy−coal flames is needed, especially with both improved kinetic mechanisms and modified physical parameters. This work presents a numerical investigation of the effects of the interaction models on the characteristics of air− and oxy−coal confined swirling flames. These interaction models are two extended eddy-dissipation models (EDMs), the finite-rate and eddy-dissipation (FRED) model and the eddy dissipation concept (EDC) model. First, two important factors were considered in the oxy−coal combustion simulations, namely, improved global reaction mechanisms and modified physical parameters. Second, with these improvements and modifications, numerical simulations of air− and oxy−coal flames were carried out. The results showed that the flames focus on the horizontal center and propagate forward with a swirling closure shape and that the flame shapes belong to an intensively accelerated flame type II. Good predictions of the combustion efficiencies were obtained by these two combustion models. Superior predictions of both the exhausted flue gas mixture and the minor carbon monoxide concentration were obtained with the eddy dissipation−chemical equilibrium (EDC) model. However, both ignition delays and temperature fields were better predicted with the kinetic-controlled and mixed-is-burned (FRED) model.

1. INTRODUCTION

CO_2 emissions from fossil-fuel-fired power plants are the major contributors to global warming. Much research has focused on reducing CO_2 emissions from power plants, and carbon capture, utilization, and storage (CCUS) technologies have been developed. In these new technologies, oxy−fuel combustion technology has been widely accepted as a promising method for a global CO_2 reduction,[1,2] which has the advantage of both cost-effectively constructing new oxy−fuel power plants and easily retrofitting traditional coal-fired power plants.

With the development of the oxy-combustion technology, the numerical simulation of oxy−fuel combustion has been a great challenge because of the complexity of the turbulence chemistry interactions. In the past two decades, numerous studies have been done on air− and oxy−coal combustion.[3−11] However, little attention has been devoted to investigate the effects of these turbulent interactions on the flame properties and behaviors, especially in oxy−coal combustion. Even fewer studies have been done on these effects with both improved global reaction mechanisms and modified physical parameters in this unconventional oxy-combustion.

In the mathematical modeling of oxy−coal swirling flames, the turbulence chemistry interactions, which are coupled with reasonable kinetic reaction mechanisms, play an important role in the numerical simulations. In previous studies,[3−6] some turbulence chemistry interaction models have been used to investigate the flame characteristics. Toporov et al.[3] investigated the stable oxy−fuel swirl flame (type II) with 21 vol% O_2 by the finite-rate and eddy-dissipation (FRED) model with a three-step reaction scheme. Some studies were presented on oxy−coal combustions using the eddy-breakup (EBU) model. Mateus[4] and Peters et al.[5] studied oxy−coal flames with three- and two-step reaction schemes, respectively. A longer ignition delay was predicted in Mateus's study.[4] Breussin et al.[6] studied oxy−natural gas flames with the EBU and EDC models and found that the equilibrium model was superior to the mixed-is-burned model. However, by some interaction models related to chemical reaction rates, some predictions could be much better if differences in the reaction mechanism between air− and oxy−fuel combustions had been considered.

Deeper understanding of the reaction mechanisms can improve the predictions by turbulence chemistry interaction models in the numerical simulation of oxy−coal flames. Based on reasonable reaction mechanisms, these interaction models can be better discussed and distinguished in terms of their effects on the flame characteristics. For oxy−coal flames, previous studies on the kinetic reaction mechanisms were reported in refs 7−11. Some articles discussed the ignition chemistry and the chemical competition of CO_2 for H through the reversible reaction CO + OH ↔ CO_2 + H. Heil et al.[7] and Glarborg and Bentzen[8] experimentally studied the burning rates of CH_4 affected by the chemical reactions of CO_2 with H. The rates of product generation and the oxidation of CO were significantly affected by CO_2 in O_2/CO_2 atmosphere. The latter also discussed the formation of CO through the reversible reaction of

Received: July 4, 2011
Accepted: November 16, 2011
Revised: October 28, 2011
Published: November 16, 2011

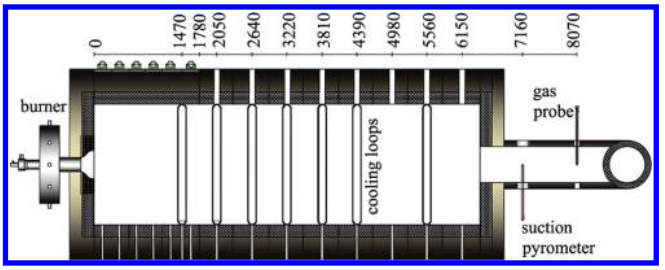

Figure 1. IFRF #1 furnace.

$CO + OH \leftrightarrow CO_2 + H$ by a detailed chemical kinetic mechanism. To obtain good predictions with global kinetic reactions, Andersen et al.[9] modified the parameters of the global chemical kinetic reactions for oxy−fuel combustions and also considered the decomposition of H_2O. Some researchers pointed out that the ignition chemistry and the burning rate can be changed by bulk CO_2. Liu et al.[10] also discussed the reaction between CO_2 and H and found this competing reaction can reduce the concentrations of radical components and the burning rates. Furthermore, in experiments on oxy−fuel combustion, Shaddix and Molina[11] showed that the devolatilization of coal particles is reduced and the ignition delay is different from conventional air combustion. The dissociation of CO_2 is very small and nearly does not affect the ignition delay at 1700 K, but the dilution and competition of CO_2 for H significantly affect the flame structure and the ignition delay.

However, both improved chemical reaction mechanisms and modified physical parameters were not comprehensively considered in some previous numerical simulations of oxy−coal flame, including CO_2 competition with O_2 for H, char gasification with CO_2 and H_2O, thermal diffusivity of CO_2, mass diffusion coefficient of O_2 and volatiles, and absorption and scattering coefficients. These chemical and physical factors significantly affect the predictions of turbulence chemistry interaction models and should be considered in the numerical simulation of oxy−fuel combustions.

Therefore, in this work, we considered both improved kinetic reaction mechanisms and modified parameters and investigated the effects on flame characteristics of two important turbulence chemistry interaction models, the FRED and EDC models. The objective was to further understand both the properties and behaviors of the oxy−coal confined swirling flame and the effects of these two interaction models, especially on flame shape, flame propagation, ignition delay, combustion efficiency, and species and temperature fields. Furthermore, these results were compared with those in both the baseline air−coal flame and the experiments of a previous work by Woycenko et al.[12] Further studies on other models used in oxy−flame numerical simulations, such as the modified radiative heat-transfer models, will be addressed in our next study. This study can help improve the understanding of oxy−coal flame characteristics and improve the research and development of oxy-burners.

2. PHYSICAL MODEL

Pilot-scale furnace #1[4] at the International Flame Research Foundation (IFRF) has an internal square cross section of 2×2 m^2 and a length of 6.25 m. Eleven independently water-cooled refractory-lined sections were installed in the furnace. Figure 1 shows the schematic geometry of the locations of cooling loops and measured points in furnace #1. A standard

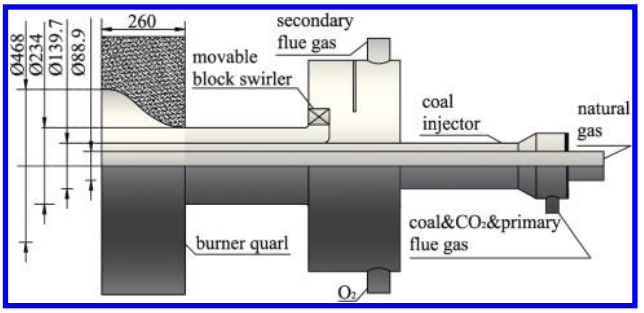

Figure 2. Aerodynamically air-staged burner.

aerodynamically air-staged burner (AASB)[4] was used in the air− and oxy−coal experiments. As shown in Figure 2, the burner was constructed of three ducts, for natural gas, primary gas with pulverized coal, and secondary flue gas. The quarl is a curved structure with vortex breakdowns that controls flame propagation and flame shape.

3. MATHEMATICAL MODEL AND PROCEDURE

3.1. Turbulent Flow Equations. The governing equations for the cases investigated in the present work are as follows

$$\frac{\partial \rho}{\partial t} + \frac{\partial}{\partial x_i}(\rho u_i) = 0 \tag{1}$$

$$\frac{\partial}{\partial t}(\rho u_i) + \frac{\partial}{\partial x_j}(\rho u_i u_j) = \frac{\partial p}{\partial x_i} + \frac{\partial}{\partial x_j}\left[\mu\left(\frac{\partial u_i}{\partial x_j} + \frac{\partial u_j}{\partial x_i} - \frac{2}{3}\delta_{ij}\frac{\partial u_i}{\partial x_j}\right)\right] + \frac{\partial}{\partial x_j}(-\rho\overline{u_i' u_j'}) \tag{2}$$

The Reynolds stress transport equation[13] is given by

$$\frac{\partial}{\partial t}(\rho\overline{u_i u_j}) + \frac{\partial}{\partial x_k}(\rho u_k \overline{u_i' u_j'}) = -\frac{\partial}{\partial x_k}[\rho\overline{u_i' u_j' u_k'} + \overline{p' u_i'}\delta_{kj} + \overline{p' u_j'}\delta_{ik}] + \frac{\partial}{\partial x_k}\left[\mu\frac{\partial}{\partial x_k}(\overline{u_i' u_j'})\right] - \rho\left(\overline{u_i' u_k'}\frac{\partial u_j}{\partial x_k} + \overline{u_j' u_k'}\frac{\partial u_i}{\partial x_k}\right) - \rho\beta(g_i\overline{u_j'\theta} + g_j\overline{u_i'\theta}) + \overline{p'\left(\frac{\partial u_i'}{\partial x_j} + \frac{\partial u_j'}{\partial x_i}\right)} - 2\mu\overline{\frac{\partial u_i'}{\partial x_k}\frac{\partial u_j'}{\partial x_k}} - 2\rho\Omega_k(\overline{u_j' u_m'}\varepsilon_{ikm} + \overline{u_i' u_m'}\varepsilon_{jkm}) + S_{user} \tag{3}$$

where the right ordinal terms of the equation are the turbulent diffusion $D_{T,ij}$, molecular diffusion $D_{L,ij}$, stress production P_{ij}, buoyancy production G_{ij}, pressure strain Φ_{ij}, dissipation ε_{ij}, production by system rotation F_{ij}, and user-defined source term S_{user}. The terms of $D_{T,ij}$, G_{ij}, Φ_{ij}, and ε_{ij} need to be modeled to close the equations.

3.2. Coupling of Continuous Turbulent Flows and Discrete Particle Trajectories. The discrete random walk model (DRWM) considers the effects of instantaneous velocity fluctuations on the particle trajectories with the stochastic methods and predicts the dispersion of particles in a continuous phase. The random velocity fluctuations are expressed as

$$u' = \varsigma\sqrt{\overline{u'^2}} \tag{4}$$

where ς is a normally distributed random number. For nonisotropy of the stresses, the values of the root-mean-square (rms)

fluctuating components are

$$u' = \varsigma\sqrt{\overline{u'^2}} \tag{5}$$

$$v' = \varsigma\sqrt{\overline{v'^2}} \tag{6}$$

$$w' = \varsigma\sqrt{\overline{w'^2}} \tag{7}$$

The characteristic lifetime of the eddy can be defined as a constant as follows

$$\tau_e = 2C_L\frac{\kappa}{\varepsilon} \tag{8}$$

where C_L is to be determined because it is not well-known. It can also be defined as a random variation r

$$\tau_e = -0.15\frac{\kappa}{\varepsilon}\log(r) \tag{9}$$

where r is a uniform random number between 0 and 1. The particle eddy crossing time is defined as

$$\tau_{cross} = -\tau\ln\left[1-\left(\frac{L_e}{\tau|u-u_p|}\right)\right] \tag{10}$$

where τ is the particle relaxation time, L_e is the eddy length scale, and $|u-u_p|$ is the magnitude of the relative velocity.

3.3. Devolatization, Char Combustion, and Chemical Kinetic Mechanism. The combustion of pulverized coal has three phases: devolatilization, endothermal volatile mixture with volume reactions, and char with particle surface reactions. In the modeling procedure, the coal particle is heated to produce a light gaseous mixture ($C_xH_yO_z$). The remained char reacts with oxidants by heterogeneous surface reactions. In the species transport equation (STE) model used in this work, we considered seven gaseous species ($C_xH_yO_z$, CO_2, CO, H_2O, O_2, H_2, N_2) and one particle species (char). The gaseous homogeneous reactions were solved by the volume reaction mechanism, and the solid heterogeneous reactions were solved by the surface reaction mechanism. Some previous works[7−11] have already discussed the kinetic reaction mechanisms in oxy−fuel combustions. These studies found that three reactions are necessary in oxy−fuel combustion, which include CO_2 competition with O_2 for H and the char gasification with CO_2 and H_2O. The four-step global chemical reaction mechanism in eqs R.1−R.4[14−16] describes the gaseous species transports, as shown in Table 1. In this mechanism, the chemical competition of CO_2 for H_2 is solved by the reverse reaction R.3.[15] The ignition chemistry is solved by reactions R.1[14] and R.4.[16] Because char gasification with H_2O and CO_2 readily occurs in the oxy−coal flames, the heterogeneous reactions R.5[17] and R.6[17] need to be considered in the reaction scheme (see Table 1). Moreover, char oxidation reaction R.7[18] was solved by the char burnout kinetic (CBK) model.[18]

The chemical percolation devolatilization (CPD) model was used to describe the devolatilization behavior of coal particles, and the CPD parameters were calculated from the proximate and ultimate analyses of the high volatile bituminous (HVB) Göttelborn coal, which was used in experiments.

The char burnout kinetic (CBK) model[18] solves the char combustion and obtains the productions of CO and CO_2. The chemical kinetic parameters in this model are expressed as

$$\ln(A) = 8.12 - 0.0715(\text{coal} - \text{coal}, \%\text{daf}) \tag{11}$$

$$q = A\exp(-E/RT_p)P_{ox}^n \tag{12}$$

$$CO/CO_2 = A_c\exp(E_c/RT_p) \tag{13}$$

where $A_c = 3.0\times10^8$, $E_c = 60$ kcal/mol, $E = 20$ kcal/mol, and $n = 0.5$, where q is the single-particle burning rate per unit external surface, in grams of carbon per second per cm^2 of external surface.

3.4. Radiation Heat-Transfer Model and Relative Modified Parameters. The discrete ordinates radiation model (DORM) solves the radiative transfer equation (RTE) as follows

$$\nabla\cdot[I(\vec{r},\vec{s})\vec{s}] + (a+\sigma_s)I(\vec{r},\vec{s}) = an^2\frac{\sigma T^4}{\pi} + \frac{\sigma_s}{4\pi}\int_0^{4\pi} I(\vec{r},\vec{s}')\,\Phi(\vec{r},\vec{s}')\,d\Omega'$$

where $\vec{r}$ is the position vector; $\vec{s}$ is the direction vector; $\vec{s}'$ is the scattering direction vector; s is the path length; a is the absorption coefficient; n is the refractive index; σ_s is the scattering coefficient; σ is the Stefan−Boltzmann constant, 5.672×10^{-8} $W/(m^2\cdot K^4)$; I is the radiation intensity, which depends on position ($\vec{r}$) and direction ($\vec{s}$); T is the local temperature; Φ is a phase function; and Ω' is a solid angle. Both the theta division Θ and the phi division φ are 4 for angular discretization.

The gaseous mixture absorption coefficients were about 0.2−0.3 and 0.4−0.5 m^{-1} in air− and oxy−coal combustion, respectively. The total pressure of H_2O and CO_2 was in the range of 0.2−0.9, and the pressure ratio between H_2O and CO_2 was about 0.125−1.0 in oxy−coal combustion.[19−24]

3.5. Conservation Equations for Chemical Species. The general form of conservation equation is

$$\frac{\partial}{\partial t}(\rho Y_i) + \nabla(\rho\vec{v}Y_i) = -\nabla\cdot\vec{J}_i + R_i + S_i \tag{15}$$

where R_i is the net rate of production of species i by chemical reaction and S_i is the rate of creation by addition from dispersed phase or others. The mass diffusion flux $\vec{J}_i$ of the ith species is expressed as

$$\vec{J}_i = -\left(\rho D_{i,m} + \frac{\mu_t}{Sc_t}\right)\nabla Y_i \tag{16}$$

where the turbulent Schmidt number, Sc_t, is 0.7. $D_{i,m}$ is the mass diffusion coefficient for the ith species.

In air atmosphere, N_2 has the highest mass fraction of all components, but in O_2/CO_2 atmosphere, CO_2 is the predominant. The mass diffusion of O_2 is different in these two different gas atmospheres. The mass diffusion coefficient, $D_{O_2,m}$, of O_2 is about 5×10^{-12} and 4×10^{-12} $kg/m^2\cdot s\cdot Pa$ for air− and oxy−coal combustion, respectively.

3.6. Energy Conservation. The energy conservation equation is expressed as

$$\frac{\partial}{\partial t}(\rho E) + \nabla\cdot[\vec{v}(\rho E + p)] = \nabla\cdot\left[k_{eff}\nabla T - \sum_j h_j\vec{J}_j + (\bar{\bar{\tau}}_{eff}\cdot\vec{v})\right] + S_h \tag{17}$$

dx.doi.org/10.1021/ie201430a |Ind. Eng. Chem. Res. 2012, 51, 691–703

Table 1. Homogeneous and Heterogeneous Reaction Kinetic Mechanism

index	reaction	A [kmol/(m^3·s)]	E (J/kmol)	ref
R.1	$C_xH_yO_z + (x-z)/2O_2 \rightarrow xCO + y/2H_2$	3.80×10^7	5.55×10^7	Shaw et al.[14]
R.2	$CO + H_2O \rightarrow CO_2 + H_2$	2.75×10^9	8.37×10^7	Jones et al.[15]
R.3	$CO_2 + H_2 \rightarrow CO + H_2O$	6.81×10^{10}	1.14×10^8	Jones et al.[15]
R.4	$H_2 + 0.5O_2 \rightarrow H_2O$	3.90×10^{17}	1.70×10^8	Hautman et al.[16]
R.5	$C + CO_2 \rightarrow 2CO$	6.35×10^{-3}	1.62×10^8	Smoot et al.[17]
R.6	$C + H_2O \rightarrow CO + H_2$	3.19×10^{-1}	2.08×10^8	Smoot et al.[17]
R.7	$(1+f)C + O_2 \rightarrow 2fCO + (1-f)CO_2$	1.07×10^1	8.368×10^4	Hurt et al.[18]

Table 2. Göttelborn Coal Proximate and Ultimate Analysis (% Dry)[a]

component	content	component	content
VM	38.2	N	1.51
FC	54.3	S	1.02
C	74.42	O	10.76
H	4.79		

[a] LCV = 30480 kJ/kg. VM = volatile matter, FC = fixed carbon, LCV = low calorific value.

Table 3. Göttelborn Coal Diameter Distribution and Mass Fraction

diameter (μm)	mass fraction (%)	diameter (μm)	mass fraction (%)
3	0.005	40	0.20
5	0.055	50	0.10
7	0.04	60	0.05
10	0.05	80	0.05
15	0.08	100	0.10
20	0.17	200	0.10

Table 4. Operating Conditions

	air-firing case		oxy-firing case	
	primary stream	secondary stream	primary stream	secondary stream
m_{gas} (kg/s)	0.15167	0.68444	0.24339	0.68444
T_K (K)	353.15	475.15	363.15	475.15
m_{coal} (kg/s)	0.07667	–	0.078333	–
Y_{O_2} (kg/kg)	0.23	0.23	0.02169	0.27347
Y_{CO_2} (kg/kg)	0.00035	0.00035	0.82611	0.46466
Y_{CO} (kg/kg)	0.0	0.0	0.0	0.00003
Y_{H_2O} (kg/kg)	0.003	0.003	0.12325	0.18706
Y_{N_2} (kg/kg)	0.76365	0.76365	0.02761	0.07295
Y_{NO} (kg/kg)	0.0	0.0	0.0013	0.0007
S	0.0	1.03	0.0	0.84

where k_{eff} is the effective conductivity, $\vec{J}_j$ is the diffusion flux of species j, and S_h includes the heat of chemical reaction and all volumetric heat sources

$$E = h - \frac{p}{\rho} + \frac{v^2}{2} \tag{18}$$

where the sensible enthalpy h is given for incompressible flows as

$$h = \sum_j Y_j h_j + \frac{p}{\rho} \tag{19}$$

where Y_j is the mass fraction of species j and h_j is defined as

$$h_j = \int_{T_{ref}}^{T} c_{p,j}\, dT \tag{20}$$

where T_{ref} equals 298.15 K.

The composition-dependent specific heat capacity can be defined as

$$c_p = \sum Y_i c_{p,i} \tag{21}$$

where Y_i is the mass fraction of the ith species and $c_{p,i}$ is the specific heat capacity of the ith species.

As the specific heat capacity of CO_2 is higher than that of N_2, the adiabatic flame temperature in an oxy−coal flame is generally no higher than that in an air−coal flame for the same thermal input. The different specific heat capacities can significantly affect the behaviors and properties of the flames.

3.7. Turbulence−Chemistry Interaction. Two important extended EDMs, namely, the FRED and EDC models, are discussed in terms of their effects on the flame characteristics in the present work. The FRED model is a kinetic-controlled and mixed-is-burned model accompanied by global chemistry. The EDC model is an eddy dissipation−chemical equilibrium model.

3.7.1. FRED Model. The FRED model considers both the finite kinetic Arrhenius rate and the mixing rates of reactants and products. The net chemistry rate is obtained from the minimum value of these parameters in this model.

3.7.1.1. Finite Kinetics Arrhenius Rate. In the finite-rate model, the chemical source term R_i is obtained from an Arrhenius kinetic equation as

$$R_i = M_{w,i} \sum_{r=1}^{N_R} \hat{R}_{i,r} \tag{22}$$

where the $M_{w,i}$ is the molecular weight of species i and $\hat{R}_{i,r}$ is the Arrhenius molar rate of creation and destruction of species i in reaction r. The rth reaction is given by

$$\sum_{i=1}^{N} \nu'_{i,r} M_i \underset{k_{b,r}}{\overset{k_{f,r}}{\rightleftharpoons}} \sum_{i=1}^{N} \nu''_{i,r} M_i \tag{23}$$

where N is the number of chemical species, $\nu'_{i,r}$ is the stoichiometric coefficient for reactant i in reaction r, $\nu''_{i,r}$ is the

dx.doi.org/10.1021/ie201430a |Ind. Eng. Chem. Res. 2012, 51, 691–703

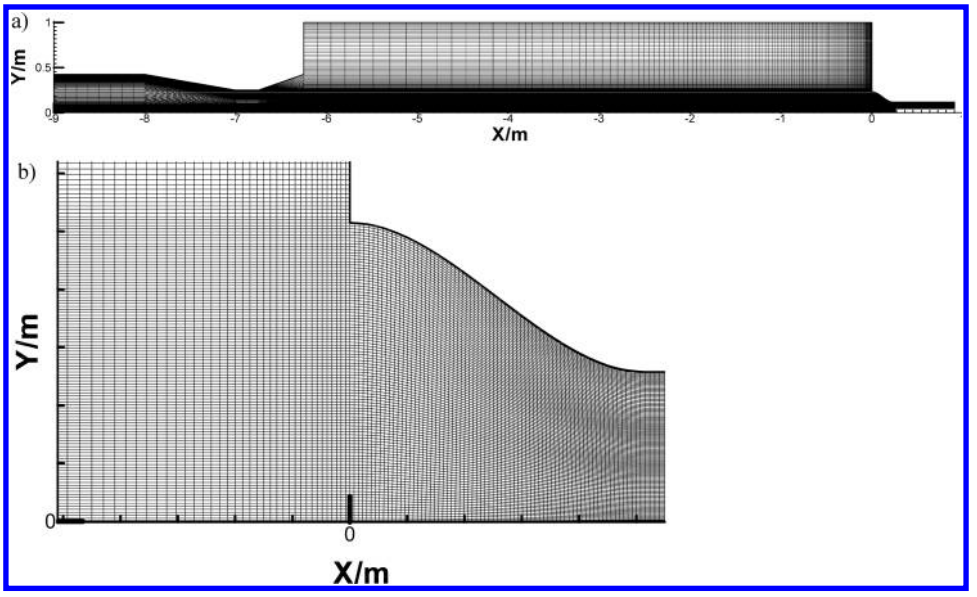

Figure 3. Body-fitted structure grid: (a) half-body grid, (b) quarl grid.

stoichiometric coefficient for product i in reaction r, M_i is a symbol for species i, $k_{f,r}$ is the forward rate constant for reaction r, and $k_{b,r}$ is the backward rate constant for reaction r. For a nonreversible reaction, the molar rate of species i in reaction r is given by

$$\hat{R}_{i,r} = \Gamma(\nu''_{i,r} - \nu'_{i,r})\left[k_{f,r}\prod_{j=1}^{N} C_{j,r}^{(\eta'_{j,r} + \eta''_{j,r})}\right] \tag{24}$$

where $C_{j,r}$ is the molar concentration of species j in reaction r, $\eta'_{j,r}$ is the rate exponent for reactant species j in reaction r, and $\eta''_{j,r}$ is the rate exponent for product species j. For a reversible reaction, the molar rate of species i in reaction r is given by

$$\hat{R}_{i,r} = \Gamma(\nu''_{i,r} - \nu'_{i,r})\left(k_{f,r}\prod_{j=1}^{N} C_{j,r}^{\eta'_{j,r}} - k_{b,r}\prod_{j=1}^{N} C_{j,r}^{\nu'_{j,r}}\right) \tag{25}$$

where $\nu'_{j,r}$ is the rate exponent for the reverse reaction and also the stoichiometric coefficient of product species j. The term Γ is a net effect of third bodies on the reaction rate and is expressed as

$$\Gamma = \sum_{j}^{N} \gamma_{j,r} C_j \tag{26}$$

where $\gamma_{j,r}$ is the third-body efficiency of the species j in reaction r. The forward rate constant $k_{f,r}$ in reaction r is

$$k_{f,r} = A_r T^{\beta_r} e^{-E_r/RT} \tag{27}$$

where A_r is the pre-exponential factor, β_r is the temperature exponent, E_r is the activation energy, and R is the universal gas constant. For a reversible reaction, the backward rate constant $k_{b,r}$ for reaction r is obtained from the forward rate constant $k_{f,r}$ as

$$k_{b,r} = \frac{k_{f,r}}{K_r} \tag{28}$$

where K_r is the equilibrium constant for reaction r and is expressed as

$$K_r = \exp\left(\frac{\Delta S_r^0}{R} - \frac{\Delta H_r^0}{RT}\right)\left(\frac{p_{atm}}{RT}\right)^{\sum_{i=1}^{N}(\nu''_{i,r} - \nu'_{i,r})} \tag{29}$$

where p_{atm} is atmospheric pressure. The term $(\Delta S_r^0/R - \Delta H_r^0/RT)$ in the exponential function is the change in Gibbs free energy, and its components are given by

$$\frac{\Delta S_r^0}{R} = \sum_{i=1}^{N}(\nu''_{i,r} - \nu'_{i,r})\frac{S_i^0}{R} \tag{30}$$

$$\frac{\Delta H_r^0}{R} = \sum_{i=1}^{N}(\nu''_{i,r} - \nu'_{i,r})\frac{h_i^0}{R} \tag{31}$$

where S_i^0 and h_i^0 are the standard-state entropy and standard-state enthalpy, respectively.

3.7.1.2. Mixing Rates of Reactants and Products. In the EDM model of Magnussen and Hjertager,[25] the net rate $R_{i,r}$ of production of the ith species in reaction r is the smaller of the two values

$$R_{i,r} = \nu'_{i,r} M_{w,i} A \rho \frac{\varepsilon}{\kappa} \min_R\left(\frac{Y_R}{\nu'_{R,r} M_{w,R}}\right) \tag{32}$$

and

$$R_{i,r} = \nu'_{i,r} M_{w,i} A B \rho \frac{\varepsilon}{\kappa}\frac{\sum_P Y_P}{\sum_j^N \nu''_{j,r} M_{w,j}} \tag{33}$$

where Y_P is the mass fraction of any product species P; Y_R is the mass fraction of the particular reactant R; and A and B are equal to 4.0 and 0.5, respectively.

3.7.2. EDC Model. The EDC model[26] is an extended model of the EDM and includes the detailed chemical mechanisms in

dx.doi.org/10.1021/ie201430a |*Ind. Eng. Chem. Res.* 2012, 51, 691–703

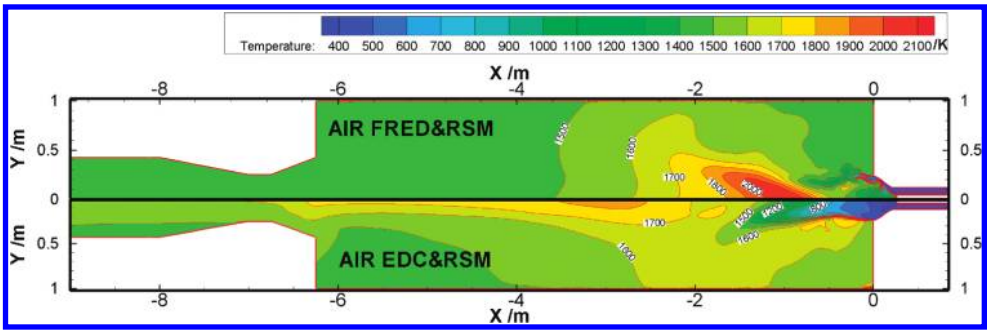

Figure 4. Temperature prediction in the air−coal case.

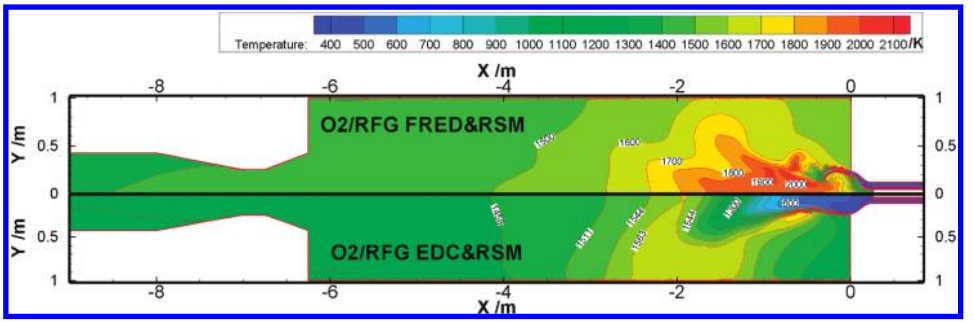

Figure 5. Temperature prediction in the oxy−coal case.

turbulent flows. The length fraction of fine scales[26,27] is expressed as

$$\xi^* = C_\xi \left(\frac{\nu\varepsilon}{\kappa^2}\right)^{1/4} \tag{34}$$

where * denotes a fine-scale quantity, C_ξ is the volume fraction constant 2.1377, and ν is the kinetic viscosity. The volume fraction of a fine scale equals ξ^{*3}. In the fine structure, the reactants are presumed to react with each other over a time scale of τ^*, as follows

$$\tau^* = C_\tau \left(\frac{\nu}{\varepsilon}\right)^{1/2} \tag{35}$$

where C_τ is the time scale constant 0.4082. The net rate R_i in the conservation eq 15 of production of the ith species is

$$R_i = \frac{\rho\xi^{*2}}{\tau^*(1-\xi^{*3})}(Y_i^* - Y_i) \tag{36}$$

where Y_i^* is the mass fraction over the time scale τ^*.

3.8. Boundary Conditions, Grid Generation, and Numerical Scheme. The boundary conditions are the same as in ref 4. Göttelborn (HVB) coal was used in the APG2 experiment. Results of the proximate and ultimate analyses are reported in Table 2. There are seven measurement holes in the wall of the horizontal furnace, and the total positions are $x/D_0 = 1-7$, where D_0 is the burner outer diameter. The coal particle diameter distribution and the mass fraction are listed in Table 3, and the operating conditions are listed in Table 4. A recycle ratio of 0.58 was used in this oxy-firing case.[4]

The axial and radial grid numbers were 343 and 115, respectively, and the total cell number was 39445, as shown in Figure 3. The refinement of grids was utilized on the furnace boundary and quarl zone. The results of this work show that the grid resolution was fine enough to obtain grid-independent results.[28] To save time, the furnace was divided into two symmetric parts by a horizontal centerline, and only one-half of the body was solved in two-dimensional space. To discuss the effects of turbulence chemistry interaction models on the flame characteristics, the present work employed the two extended EDMs with the Reynolds stress model (RSM) in the air− and oxy−coal cases. The pressure−velocity coupling[29] was solved by the semi-implicit method for pressure-linked equations (SIMPLE) algorithm.

4. RESULTS AND DISCUSSION

The cubic equation fits the curved quarl, which modifies the streams with less eddy formation in the quarl structure (see Figure 3). This curved quarl modifies the flame shape and flame propagation in the highly confined horizontal furnace. As a result of this mathematical modeling of the air− and oxy−coal confined swirling flames, within the quarl structure, the combustive mixture is not heated sufficiently by radiative heat transfer and convection from the surrounding gaseous mixture and walls. Accordingly, the secondary streams near the quarl wall are heated slowly, and the ignition delays increase (see Figures 4 and 5). However, in the corresponding experiments, the ignition chemistry had already arisen in the quarl structure, and the flame maximum temperature had already reached about 2100 K within the internal recirculation zone (IRZ) (see Figures 6 and 7).

4.1. Combustion Characteristics. In both air− and oxy−coal flames, confined swirling flames with large momentums mainly focus on the horizontal centerline in the furnace, the flame propagates forward, and the flame shapes are similar to the closed flame structure, belonging to intensively accelerated flame type II[30] (see Figures 4 and 5). The reason is that the limited and accelerated gaseous mixture is injected from a highly confined

dx.doi.org/10.1021/ie201430a |*Ind. Eng. Chem. Res.* 2012, 51, 691–703

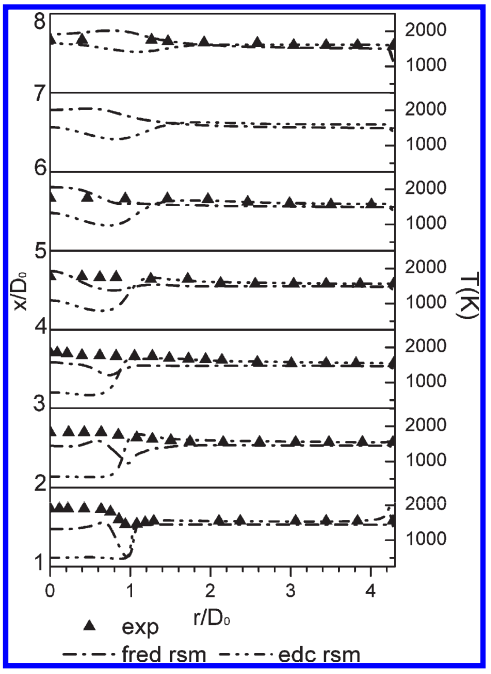

Figure 6. Temperature profiles in the air−coal case.

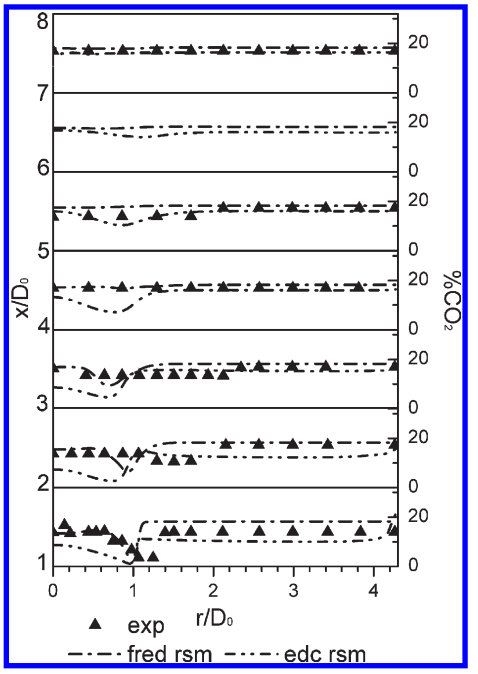

Figure 8. CO_2 profiles in the air−coal case.

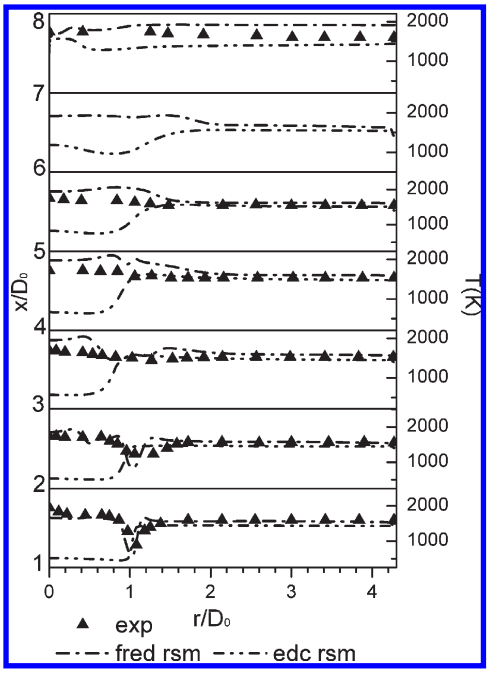

Figure 7. Temperature profiles in the oxy−coal case.

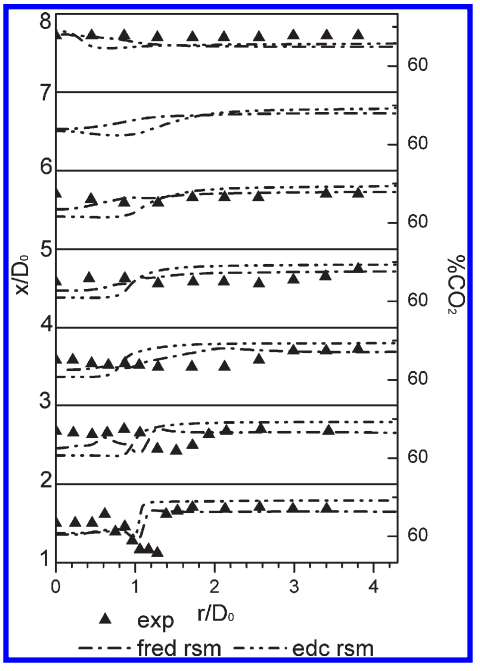

Figure 9. CO_2 profiles in the oxy−coal case.

structure. In particular, a curved quarl with zero angles at its inlet and outlet can effectively control the direction of the swirling flames. The EDC model gives longer ignition delays, and the high temperature focuses at about x/D_0 = 7.0 for both the air− and oxy−coal flames. However, the FRED model obtains shorter ignition delays and the high temperature just in the quarl. This high temperature in the quarl can further improve flame stability and coal particle burnout.

4.2. Temperature Characteristics. In both air− and oxy−coal cases, shown in Figures 6 and 7, the temperatures predicted by the EDC model are significantly lower than those from the experimental measurements in the center zone of the furnace. However, the temperature fields predicted by the FRED model are nearly in agreement with those from the detailed measurements, and the high-temperature zone is close to the burner outlet in the quarl. In these two experiments, the temperature fields are similar to each other in the furnace, which shows that the swirling burner can work well for the requirements of similar flames. These obtained similar temperature fields can effectively enhance the similarity of the combustion characteristics in the air− and oxy−coal flames.

dx.doi.org/10.1021/ie201430a |*Ind. Eng. Chem. Res.* 2012, 51, 691–703

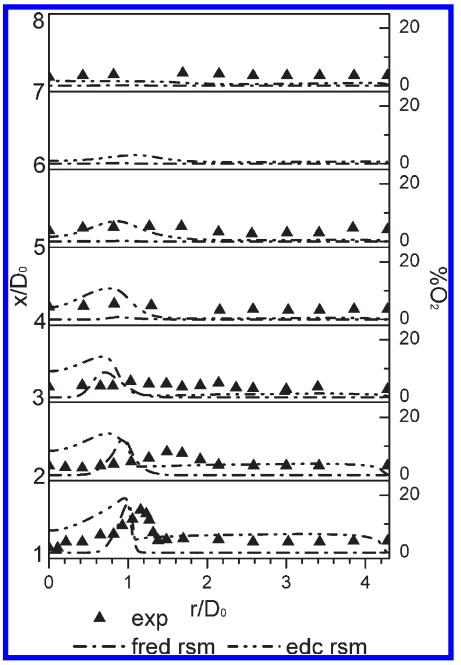

Figure 10. O_2 profiles in the air−coal case.

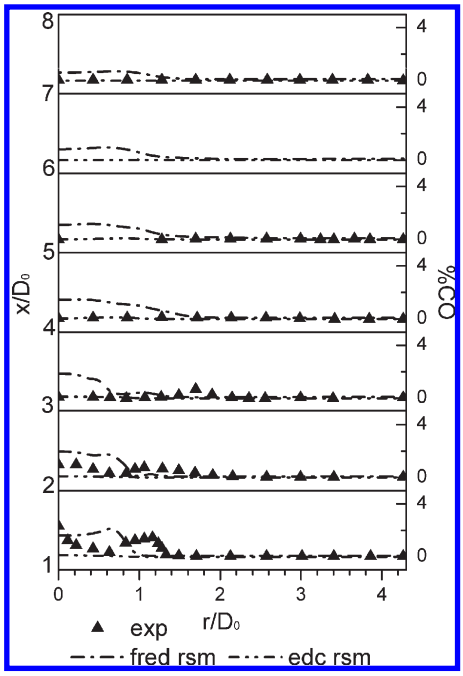

Figure 12. CO profiles in the air−coal case.

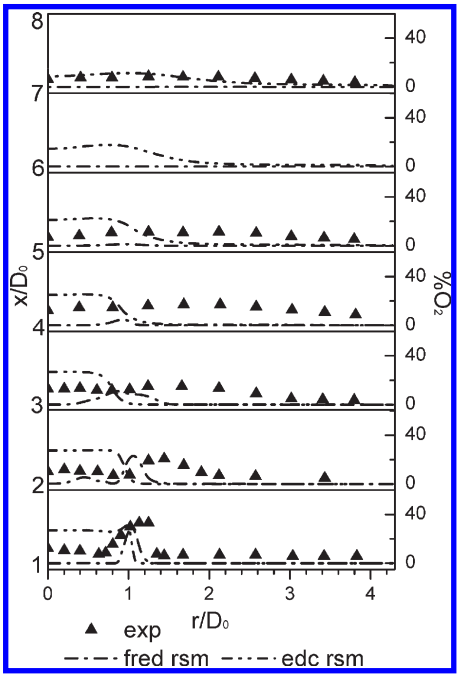

Figure 11. O_2 profiles in the oxy−coal case.

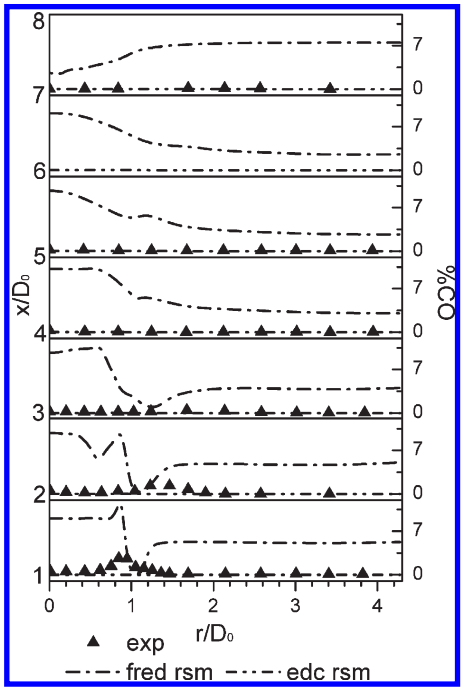

Figure 13. CO profiles in the oxy−coal case.

4.3. Carbon Dioxide Characteristics. In the primary burning zone, especially in the IRZ, the high temperature enhances the release and burning of the volatile mixture. The flame stability is kept with a high concentration of CO_2, at 17% (see Figure 8) in the air−coal flame and 83% (see Figure 9) in the oxy−coal flame. Because of the low temperature in the range $r/D_0 = 0.5-1.5$, the chemical reaction rates of the mixture decrease, including the oxidation rates of volatile matter and char, and lower amounts of CO_2 are produced near the quarl wall. However, the two turbulent combustion models, FRED and EDC, give good predictions of CO_2 at large radial distances $r/D_0 \geq 1.5$ for the two cases.

4.4. Oxygen Characteristics. For the air− and oxy−coal flames, the exhausted volume fractions of oxygen are 2.1% and 3.9%, respectively (see Figures 10 and 11). The excess air ratio can enhance the stability of the swirling flame and improve the burnout ratio in the furnace. Within the IRZ, near the outlet of the quarl, turbulent reactions consume the bulk of oxygen. In the radial range of $0.5 \leq r/D_0 \leq 1.5$, the lower temperature makes the chemical activities of reactants decrease, and the actual

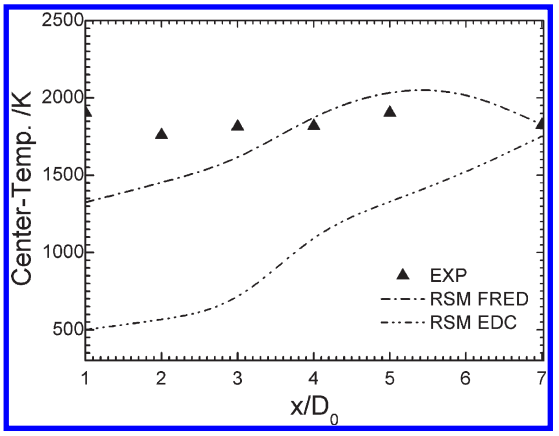

Figure 14. Center temperature profiles in the air−coal case.

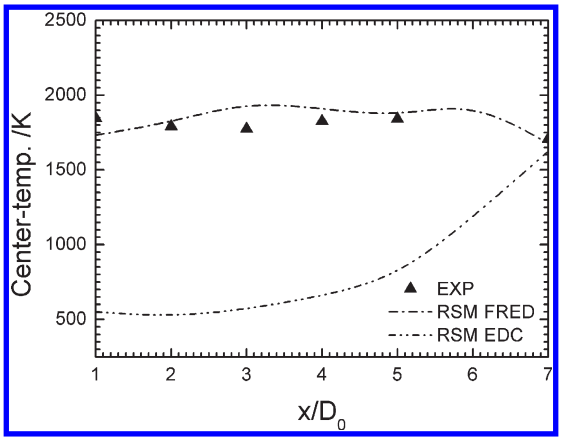

Figure 15. Center-T profiles in the oxy−coal case.

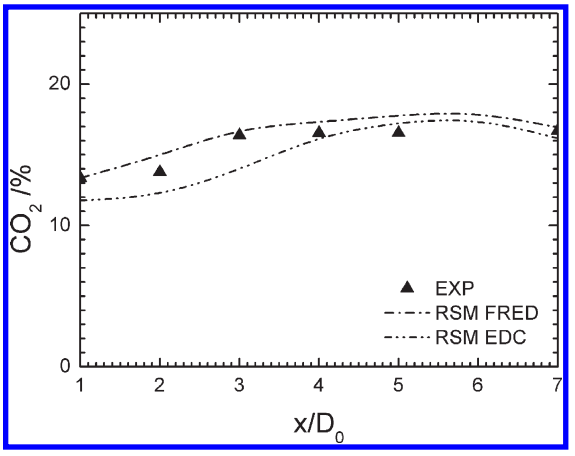

Figure 16. Center CO_2 profiles in the air−coal case.

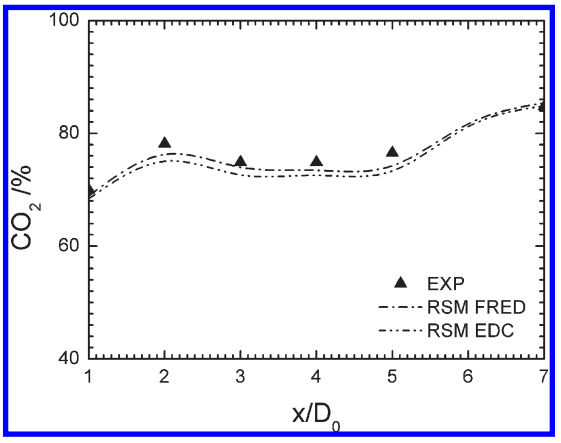

Figure 17. Center CO_2 profiles in the oxy−coal case.

consumption of oxygen in the furnace is lower. For the two turbulent combustion models, the predictions for oxygen are in agreement with the experimental results at $r/D_0 \geq 1.5$. In the primary burning zone, the kinetic-controlled and mixed-is-burned (FRED) model gives better predictions for oxygen. However, the eddy dissipation−chemical equilibrium (EDC) model gives higher results for oxygen because of the reduced chemical activities of the reactants at lower temperature.

4.5. Carbon Monoxide Characteristics. For the oxy−coal flame, both the Boudouard reaction (R.5) and the gasification reaction (R.6) significantly affect the production of CO (see Figure 13), especially in fuel-rich zones. In the reduction zone, near the jets of secondary streams, the Boudouard reaction (R.5) is enhanced with the bulk of the flue gas mixture, and a local peak is formed at $r/D_0 \leq 1.5$, shown in Figures 12 and 13. The concentration of CO in the exhausted flue gas is nearly the same, at 0.06% and 0.08% for air− and oxy−coal flame, respectively. The eddy dissipation−chemical equilibrium model (EDC) gives better predictions for the concentration of CO in the furnace. A partial reason for this is that the chemical equilibrium components are solved by chemical reaction rates in the fine structure. Another reason is that the oxidation of H_2 by CO_2 is considered in reaction R.3, which is obtained from the reaction R.2 by chemical equilibrium.

4.6. Temperature Characteristics through the Centerline. Figures 14 and 15 show that the temperature through the centerline changes with the combustion model in both air− and oxy−coal flames. The ignition chemistries occur in the quarl structure, and the recycled flue gas mixture with a maximum temperature lies in the IRZ for both flames. However, the EDC model gives greater ignition delays for both air− and oxy−coal flames, and the lower center temperatures significantly affect the pulverized coal combustion. At the outlet of the furnace, the predicted gaseous temperatures are nearly the same for the two flames. For the air−coal flame, the predicted temperatures at $x/D_0 = 1.0$ are 1300 and 500 K for the FRED model and the EDC model, respectively (see Figure 14). For the oxy−coal flame, the intense chemical reactions remain in the outlet of the quarl. However, the EDC model gives a lower temperature field, and the maximum difference between measurement and prediction is about 1400 K (see Figure 15). In the experiments, the intense chemical reactions remain in the outlet of the burner, and high temperatures are reached in the quarl for both flames. The reason is that internal recycled flue gas mixture with a high temperature ignites the volatile mixture in the quarl.

4.7. Carbon Dioxide Characteristics through the Centerline. Figures 16 and 17 show that the released CO_2 through the centerline is steady and continuous in both air− and oxy−coal flames. This demonstrates that the flame stability is retained in a high concentration of CO_2 and that the ignition chemistry occurs in furnace. The two combustion models, the FRED and EDC models, give similar predictions of CO_2 for each case, especially

dx.doi.org/10.1021/ie201430a |*Ind. Eng. Chem. Res.* 2012, 51, 691–703

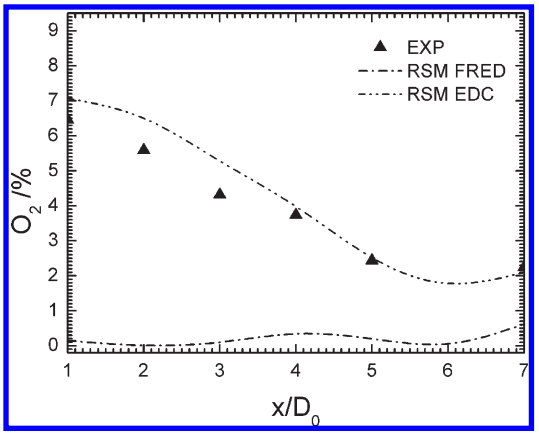

Figure 18. Center O_2 profiles in the air−coal case.

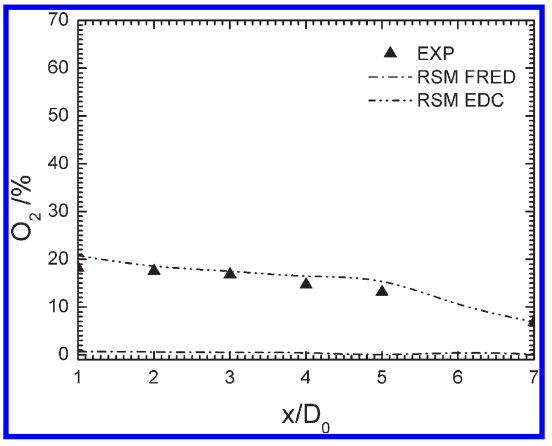

Figure 19. Center O_2 profiles in the oxy−coal case.

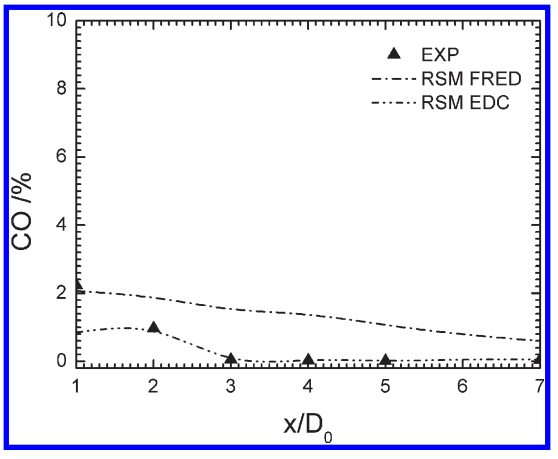

Figure 20. Center CO profiles in the air−coal case.

for $x/D_0 \geq 4.0$. In oxy−coal combustion, with high concentrations of CO_2 (82.8%) and H_2O (estimated 25%), turbulent combustion is significantly affected by both the specific heat capacity of CO_2 and the latent heat of H_2O.

4.8. Oxygen Characteristics through the Centerline. Figures 18 and 19 show that excess oxygen remains at the centerline in both air− and oxy−coal flames. In air−coal combustion, the

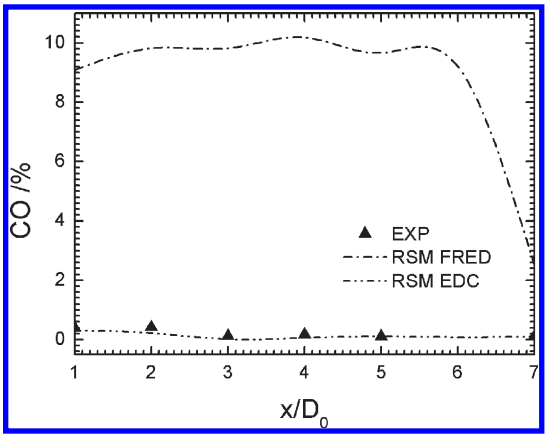

Figure 21. Center CO profiles in the oxy−coal case.

Table 5. Comparison between Experimental Measurements and Numerical Predictions

		air−coal			oxy−coal		
adiabatic flame temperature (K)		2376			2360		
thermal input (kW)		2497			2467		
		expt	FRED	EDC	expt	FRED	EDC
flue gas temperature (K)		1355	1410	1420	1402	1400	1405
combustion efficiency (%)		99.4	99.8	99.9	99.8	99.3	99.9
exhausted flue gas (dry %)	O_2	2.1	0.4	2.0	3.9	1.4	3.0
	CO	0.06	0.48	0.06	0.08	2.51	0.08
	CO_2	16.6	17.7	16.4	82.8	82.5	83.6

reactants consist of pulverized coal and air, whereas in oxy−coal combustion, the reactants consist of pulverized coal, recycled flue gas (RFG), and pure oxygen. In oxy−coal combustion, pure oxygen is injected into the secondary stream. Accordingly, the combustion aerodynamic field can be affected by this injection of pure oxygen because it can affect the combustion accelerated stream. Figure 18 shows that the excess oxygen is about 2.0−7.0% at the centerline, but Figure 19 shows that the excess O_2 is about 5.0−20.0% at the centerline. In the primary and secondary streams, the oxygen partial pressures are 2.5% and 26.6%, respectively. Correspondingly, the partial pressures of gaseous water are 25.1% and 32.4%, respectively. The total partial pressure of oxygen is 15.5%, and the total partial pressure of gaseous water is 18.6% in the oxy−coal combustion. In this wet recirculation combustion system, the oxygen partial pressure is 26.6% in the secondary stream, and the excess oxygen is about 4.0% in the exhausted flue gas. These two factors improve the flame stability and the flame characteristics, namely, similar temperature, high burnout ratio, and even reduced ignition delay. The eddy dissipation−chemical equilibrium, EDC, model gives good predictions for oxygen at the centerline of the furnace.

4.9. Carbon Monoxide Characteristics through the Centerline. Figures 20 and 21 show small concentrations of CO for both the air− and oxy−coal flames at the centerline of the furnace. In oxy−coal combustion, the CO enhances the ignition chemistry and the NO reduction near the quarl. At the outlet of the confined quarl, the concentrations of CO predicted by the EDC model are similar to those obtained by measurements for both flames. As shown in Figures 20 and 21, the eddy

dx.doi.org/10.1021/ie201430a |*Ind. Eng. Chem. Res.* 2012, 51, 691–703

dissipation−chemical equilibrium (EDC) model gives an exact prediction of CO, but the kinetic-controlled and mixed-is-burned (FRED) model gives an upper prediction.

4.10. Comparisons between Measurements and Predictions. To maintain similar radiative and convective heat-transfer characteristics for air− and oxy−coal flames, the thermal input keeps nearly the same value of 2480 kW, and the adiabatic temperature in both cases is about 2370 K (see Table 5). Accordingly, the similar temperature distributions and similar aerodynamic flow fields even enhance the similar flame properties and behaviors, including flame shape, flame propagation, and burnout ratio. It is important that similar flame characteristics are kept for air− and oxy−coal flames, because minimal changes are needed for new or reconstructed oxy−coal power plants.

In both flames, the combustion efficiencies are more than 99.0%, and good burnout ratios can be obtained for this swirling burner. In the exhausted flue gas mixture, the concentrations of CO_2 are 16.6% and 82.8% for the air− and oxy−coal flames, respectively (see Table 5). It is demonstrated that stable combustion can be obtained even at high concentrations of CO_2 for an oxy−coal flame. Both turbulent combustion models can correctly predict the combustion efficiencies and concentrations of the exhausted flue gas mixture.

5. CONCLUSIONS

The present work has comprehensively considered improved chemical reaction mechanisms and modified physical parameters, including CO_2 competition with O_2 for H, char gasification with CO_2 and H_2O, thermal diffusivity of CO_2, mass diffusion coefficient of O_2 and volatiles, and absorption and scattering coefficients. Based on these improved and modified factors, investigations on the effects of the two extended EDMs, namely, the FRED and EDC models, on the flame characteristics were carried out. This work can help bring about further understanding of oxy−coal flame characteristics and assist the design of new oxy-burners.

The conclusions are as follows:

In the air− and oxy−coal flames, the flame focuses on the horizontal center in the furnace, and the flame propagates forward with a swirling closure structure. The air− and oxy−coal confined swirling flames are similar to each other, and the two adiabatic flame temperatures are nearly the same, which shows that this burner can satisfy the requirements of multiple flames.

In the air− and oxy−coal flames, the flame shapes can be classified as intensively accelerated flame type II, which are affected by a highly confined quarl structure. The quarl constructs a confined curve structure with vortex breakdowns and controls the flame propagation and shape.

In the air− and oxy−coal flames, high combustion efficiencies are obtained by both combustion models, namely, the FRED and EDC models. Good predictions between the carbon monoxide fields and the exhausted flue gas mixture are obtained by the EDC model coupled with a chemical equilibrium procedure. The temperature fields and ignition delays are better solved by the FRED model accompanied by a global chemistry.

AUTHOR INFORMATION

Corresponding Author

*E-mail: liujingzhang2005@163.com. Tel.: +86-27-8754-2417. Fax: +86-27-8754-5526.

ACKNOWLEDGMENT

The authors gratefully acknowledge financial support from the National Key Basic Research and Development Program (Grant 2011CB707300), National High Technology Research and Development of China (Grant 2009AA05Z315), National Natural Science Foundation (Grant 50936001), and National Key Technology Research and Development Program (Grant 2011BAC0500).

NOMENCLATURE

AASB = aerodynamically air-staged burner
CBK = char burnout kinetic model
CCS = carbon capture and storage
CPD = chemical percolation devolatilization
DORM = discrete ordinates radiation model
DRWM = discrete random walk model
DTRM = discrete transfer radiation model
EBU = eddy breakup model
EDC = eddy-dissipation concept model
EDM = eddy-dissipation model
FRED = finite-rate and eddy-dissipation
HVB = high volatile bituminous
IFRF = International Flame Research Foundation
IRZ = internal recirculation zone
RANS = Reynolds-averaged Navier−Stokes
RFG = recycled flue gas
rms = root mean square
RSM = Reynolds stress model
RTE = radiative transfer equation
SIMPLE = semi-implicit method for pressure-linked equation
STE = species transport equation
STM = species transport model

Scalars

A = constant value of 4.0, pre-exponential factor
A_c, A_r = pre-exponential factors
B = constant value of 0.5
$C_{j,r}$ = molar concentration of species j in reaction r
C_ξ = volume fraction constant equal to 2.1377
C_τ = time scale constant equal to 0.4082
$D_{T,ij}$ = turbulent diffusion
$D_{L,ij}$ = molecular diffusion
$D_{i,m}$ = mass diffusion coefficient of species i ($kg/m^2 \cdot s \cdot Pa$)
D_0 = burner outer diameter (m)
E, E_c = activation energies (kJ/kg)
F_{ij} = production by system rotation
f = coefficient for chemical formula
G_{ij} = buoyancy production
h = sensible enthalpy (kJ/kg)
h_i^0 = standard-state enthalpy (kJ/kg)
$k_{b,r}$ = backward rate constant for reaction r
k_{eff} = effective conductivity
$k_{f,r}$ = forward rate constant for reaction r
K_r = equilibrium constant for reaction r
L_e = eddy length scale
M_i = symbol for species i
$M_{w,i}$ = molecular weight of species i
n = refractive index
N = number of chemical species
p_{atm} = atmospheric pressure (1.01×10^5 Pa)
P_{ij} = stress production

q = single burning rate per unit external surface {g of carbon/[s·(cm^2 of external surface)]}
R = universal gas constant [8.3145 J/(mol·K)]
R_i = net rate of production of species i
$\hat{R}_{i,r}$ = Arrhenius molar rate of species i
s = path length
S_i^0 = standard-state entropy (kJ/kg·K)
S_{user} = user-defined source term
Sc_t = turbulent Schmidt number
u' = random fluctuation in the x velocity (m/s)
v' = random fluctuation in the y velocity (m/s)
w' = random fluctuation in the z velocity (m/s)
Y_i^* = fine-scale species mass fraction
Y_j = mass fraction of species j
Y_P = mass fraction of the product species P
Y_R = mass fraction of the particular reactant R

Vectors

$\vec{J}_i$ = mass diffusion flux of species i
$\vec{r}$ = position vector
$\vec{S}$ = direction vector
$\vec{S}'$ = scattering direction vector

Greek Letters

α = absorption coefficient (m^{-1})
$\gamma_{j,r}$ = third-body efficiency of species j in reaction r
Γ = net effect of third bodies
ε_{ij} = turbulent dissipation
ζ = normally distributed random number
$\eta'_{j,r}$ = rate exponent for reactant species j in reaction r
$\eta''_{j,r}$ = rate exponent for product species j in reaction r
Θ = theta division
I = radiation intensity
ν = kinetic viscosity (m^2/s)
$\nu'_{i,r}$ = stoichiometric coefficient for reactant i in reaction r
$\nu''_{i,r}$ = stoichiometric coefficient for product i in reaction r
ξ^{*3} = volume fraction of a fine scale
σ_s = scattering coefficient (m^{-1})
σ = Stefan−Boltzmann constant, 5.672×10^{-8} W/m^2·K^4
τ = particle relaxation time
τ^* = time scale
τ_{cross} = eddy crossing time
τ_e = eddy lifetime
Φ = phi division or phase function
Φ_{ij} = pressure strain
Ω' = solid angle

Subscripts

i, j, k = coordinate directions

REFERENCES

(1) Toftgaard, M. B.; Brix, J.; Jensen, P. A.; Glarborg, P.; Jensen, A. D. Oxy−Fuel Combustion of Solid Fuels. *Prog. Energy Combust.* **2010**, *36* (5), 581–625.

(2) Buher, B. J. P.; Elliott, L. K.; Sheng, C. D.; Gupta, R. P.; Wall, T. F. Oxy−Fuel Combustion Technology for Coal-Fired Power Generation. *Prog. Energy Combust.* **2005**, *31* (4), 283–307.

(3) Toporov, D.; Bocian, P.; Heil, P.; Kellermann, A.; Stadler, H.; Tschunko, S.; Förster, M.; Kneer, R. Detailed Investigation of a Pulverized Fuel Swirl Flame in CO_2/O_2 Atmosphere. *Combust. Flame* **2008**, *155* (4), 605–618.

(4) Mateus, A. R. Analysis of Radiation Properties of Gases and Utilization in a Pulverized Coal Combustion Simulation Model. *Dissertation*, Instituto Superior Tecnico, Lisbon, Portugal, 2007.

(5) Andre, A. F. P.; Roman, W. Mathematical Modeling of 2.4MW Swirling Pulverized Coal Flame. *Combust. Sci. Technol.* **1997**, *122* (1), 131–182.

(6) Breussin, F.; Lallemant, N.; Roman, W. Computing of Oxy−Natural Gas Flames Using Both a Global Combustion Scheme and a Chemical Equilibrium Procedure. *Combust. Sci. Technol.* **2000**, *160* (1), 369–397.

(7) Heil, P.; Toporov, D.; Förster, M.; Kneer, R. Experimental Investigation on the Effect of O_2 and CO_2 on Burning Rates during Oxyfuel Combustion of Methane. *Proc. Combust. Inst.* **2011**, *33* (2), 3407–3413.

(8) Glarborg, P.; Bentzen, L. Chemical Effects of a High CO_2 Concentration in Oxy−Fuel Combustion of Methane. *Energy Fuels* **2008**, *22* (1), 291–296.

(9) Andersen, J.; Rasmussen, C. L.; Giselsson, T.; Glarborg, P. Global Combustion Mechanisms for Use in CFD Modeling under Oxy−Fuel Conditions. *Energy Fuels* **2009**, *23* (3), 1379–1389.

(10) Liu, F.; Guo, H.; Smallwood, G. J. The Chemical Effect of CO_2 Replacement of N_2 in Air on the Burning Velocity of CH_4 and H_2 Premixed Flames. *Combust. Flame* **2003**, *133* (4), 495–497.

(11) Shaddix, C. R.; Molina, A. Particle Imaging of Ignition and Devolatilization of Pulverized Coal during Oxy−Fuel Combustion. *Proc. Combust. Inst.* **2009**, *32* (2), 2091–2098.

(12) Woycenko, D. M.; van de Kamp, W. L.; Roberts, P. A. *Combustion of Pulverized Coal in a Mixture of Oxygen and Recycled Flue Gas*; Report F98/Y/2; International Flame Research Foundation (IFRF): Livorno, Italy, 1995.

(13) Launder, B. E.; Reece, G. J.; Rodi, W. Progress in the Development of a Reynolds-Stress Turbulence Closure. *J. Fluid Mech.* **1975**, *68* (3), 537–566.

(14) Shaw, D.; Zhu, X.; Misra, M.; Essenhigh, R. Determination of a Global Kinetics of Coal Volatiles Combustion. *23rd Symp. (Int.) Combust.* **1990**, 1155–1162.

(15) Jones, W. P.; Lindstedt, R. P. Global Reaction Schemes for Hydrocarbon Combustion. *Combust. Flame* **1988**, *73* (3), 233–249.

(16) Hautman, D. J.; Dryer, F. L.; Schug, K. P.; Glassman, I. A Multiple-Step Overall Kinetic Mechanism for the Oxidation of Hydrocarbon. *Combust. Sci. Technol.* **1981**, *25* (5), 219–235.

(17) Smoot, D.; Pratt, D. *Pulverized Coal Combustion and Gasification Theory and Applications for Continuous Flow Processes*; Plenum Press: New York, 1979.

(18) Hurt, R.; Sun, J. K.; Lunden, M. A Kinetic Model of Carbon Burnout in Pulverized Coal Combustion. *Combust. Flame* **1998**, *113* (2), 181–197.

(19) Smith, T. F.; Shen, Z. F.; Friedman, J. N. Evaluation of Coefficients for the Weighted Sum of Gray Gases Model. *ASME J. Heat Transfer* **1982**, *104* (4), 602–608.

(20) Johansson, R.; Andersson, K.; Leckner, B.; Thunman, H. Models for Gaseous Radiative Heat Transfer Applied to Oxy−Fuel Conditions in Boilers. *Int. J. Heat Mass Transfer* **2010**, *53* (1), 220–230.

(21) Kangwanpongpan, T.; Corrêa da Silva, R.; Tappe, S.; Klatt, M.; Krautz, H. J. Numerical Comparison of Spectral Non-Gray Gases Modeling in a Swirling Oxyfuel Burner. Presented at the *35th International Technical Conference on Coal Utilization & Fuel Systems*, Clearwater, Florida, USA, June 6−10, 2010.

(22) Rehfeldt, S.; Kuhr, C.; Ehmann, M.; Bergins, C. Modeling of Radiative Heat Transfer in an Oxyfuel Atmosphere with a Wide Band Model and a Weighted Sum of Gases. Presented at the *35th International Technical Conference on Coal Utilization & Fuel Systems*, Clearwater, Florida, USA, June 6−10, 2010.

(23) Kangwanpongpan, T.; Krautz, H. J. Numerical Simulation of Lignite Combustion in O_2/CO_2 Environment by Eddy-Dissipation Model. Presented at the *First International Oxyfuel Combustion Conference*, Cottbus, Germany, September 7−11, 2009.

(24) Liu, Z. H. *Model Development for Predicting Pulverized Coal Combustion and Ash Deposition*; First Year Report, Lisbon University, Portugal; 2004.

(25) Magnussen, B. F.; Hjertager, B. H. On Mathematical Models of Turbulent Combustion with Special Emphasis on Soot Formation and Combustion. Presented at the *16th Symposium (International) on Combustion*, Cambridge, Massachusetts, USA, August 15−20, 1976.

(26) Magnussen, B. F. On the Structure of Turbulence and a Generalized Eddy Dissipation Concept for Chemical Reaction in Turbulent Flow. Presented at the *9th AIAA Meeting*, St. Louis, MO, January 12−15, 1981.

(27) Gran, I. R.; Magnussen, B. F. A Numerical Study of a Bluff-Body Stabilized Diffusion Flame. Part 2. Influence of Combustion Modeling and Finite-Rate Chemistry. *Combust. Sci. Technol.* **2007**, *19* (1), 191–217.

(28) Faltsi-Saravelou, O.; Wild, P.; Sazhin, S. S.; Michel, J. E. Detailed Modeling of a Swirling Coal Flame. *Combust. Sci. Technol.* **1997**, *123* (1), 1–22.

(29) Vandoormaal, J. P.; Raithby, G. D. Enhancements of the SIMPLE Method for Predicting Incompressible Fluid Flows. *Num. Heat Transfer* **1984**, *7* (2), 147–163.

(30) Roman, W.; Jacques, D. Combustion Accelerated Swirling Flows in High Confinements. *Prog. Energy Combust.* **1992**, *18* (4), 349–367.